

Adsorption and Structure of Octadecanethiol on Zinc Surfaces As Probed by Sum Frequency Generation Spectroscopy, Imaging, and Electrochemical Techniques

Jonas Hedberg,^{*,†} Christofer Leygraf,[†] Katherine Cimatu,[‡] and Steven Baldelli[‡]

Department of Chemistry, Division of Corrosion Science, Royal Institute of Technology, Drottning Kristinas v. 51, SE-100 44 Stockholm, Sweden, and Department of Chemistry, University of Houston, Houston, Texas 77204-5003

Received: July 6, 2007; In Final Form: September 7, 2007

Octadecanethiol (ODT) adsorbed onto zinc has been studied with sum frequency generation (SFG), sum frequency generation imaging microscopy (SFG-IM), X-ray photoelectron spectroscopy (XPS), cyclic voltammetry (CV), and electrical impedance spectroscopy (EIS) in order to investigate its corrosion protective ability and conformational ordering. SFG shows that ODT forms an ordered adsorbate on both reduced and oxidized zinc within short times after immersion in 1 mM ODT/ethanol solution. The corrosion protection, deduced by EIS, is also improved after immersion in the ODT solution. After longer immersion times, the corrosion protection decreases as well as the conformational order of the adsorbed ODT. Increasing the ODT concentration avoids this degradation with prolonged immersion time. The ODT is seen in the XPS spectra to adsorb to the reduced as well as the oxidized zinc by forming a Zn–S bond for both short and long immersion times. The SFG-IM completes the picture, showing a heterogeneous surface with areas corresponding to ordered ODT as well as disordered or uncovered regions. The density of adsorbed ODT after 24 h immersion time for both reduced and oxidized zinc was deduced from CV and was found to be approximately 6.7×10^{-9} mol/cm².

1. Introduction

An important aspect of organic coatings on metals is the phase boundary between the metal and the coating. Adhesion and chemical bonds are of utmost importance, and the properties of these are closely related to interfacial properties, such as corrosion protection ability. In modern surface technology, it is desired to apply ultrathin corrosion protecting films on common metals, such as steel, galvanized steel, and aluminum, within very short timescales. A potential model for surface modifications of metals is an alkanethiol, CH₃(CH₂)_nSH, which consists of a long hydrocarbon chain with a sulfur head group and serves as a widely used molecule for model studies of self-assembled monolayers, with gold being the most common substrate.¹

Thiols adsorbed on oxidized metals have been studied, though not as extensively as gold, and include substrates such as tin,² copper,^{3,4} silver,⁵ iron,^{6,7} and zinc.^{8,9} Thiols adsorb on the metal surface by formation of a metal–sulfur bond. Thus, it is somewhat surprising that alkanethiols are able to form ordered monolayers on oxide surfaces. Presumably, the mechanism of adsorption is that of dissociation, where the oxygen and hydroxide groups are desorbed when the thiol is adsorbed to the metal atom. The fact that the thiol is mainly coordinated to the metal atoms in the oxide is suggested by X-ray photoelectron spectroscopy (XPS) data, whereby zinc terminated ZnO has been shown to adsorb ethanethiol and methanethiol dissociatively.^{10–12} It has been shown with temperature programmed desorption that the thiol reduces the oxygen at the surface and forms a zinc–

sulfur bond. O-polar ZnO, on the other hand, only adsorbs the thiols molecularly at room temperature. A further aspect of thiols has been the growth inhibition of ZnO nanoparticles, by adsorbing and effectively limiting further growth.^{13,14}

This study aims at exploring the adsorption of octadecanethiol (ODT, CH₃(CH₂)₁₇SH) on oxidized and reduced zinc surfaces with a multianalytical approach. Particular emphasis is on the structure of the adsorbate and how it relates to the corrosion protection ability. The techniques include molecular level investigations using sum frequency generation vibrational spectroscopy (SFG) and XPS and macroscopic methods such as electrochemical impedance spectroscopy (EIS) and cyclic voltammetry (CV). In addition, the use of SFG imaging provides spatially resolved spectroscopy that is useful in interpreting the homogeneity of the surface.

2. Experimental Section

The outline of the experimental procedure is as follows: first, the electrode was polished and then transferred to the electrochemical cell, where the electrochemical reduction was performed to remove residual oxidized species. If an oxidized substrate was to be studied, the oxidation was performed immediately following the reduction step. The immersion into the thiol solution followed next, and finally the electrode was transferred to the appropriate experiment (SFG, EIS, CV, or XPS), which was performed directly after the sample preparation. The experiments were repeated at least three times.

2.1. Materials. A 7 mm diameter zinc rod (99.999%) was obtained from Goodfellow. The chemicals used were octadecanethiol (herein shortened ODT, CH₃(CH₂)₁₇SH, 98%, purchased from Aldrich), ethanol (99.5%, Prolab), acetone (99%, Alfa Aesar), NaOH (98%, Eka Nobel), LiCl (99.9%, Aldrich), and NaClO₄ (99%, Aldrich).

* To whom correspondence should be addressed. E-mail: jhed@kth.se. Fax: +46 8 208284.

[†] Royal Institute of Technology.

[‡] University of Houston.

2.2. Sample Preparation. The zinc electrodes were abraded with SiC grit paper, starting from 500 mesh in steps down to 4000 mesh. Diamond polishing was subsequently applied with particle size 6, 3, 1, and finally 0.25 μm . In order to remove the residual diamond particles, the zinc electrode was sonicated in ethanol for 5 min between each diamond polishing step. After the final polishing step, the zinc electrode was sonicated in acetone for 10 min and finally rinsed with ethanol and water. The water was obtained from a Millipore RiOs-8 and Milli-Q PLUS purification system and filtered through a 0.2 μm Millipak filter. The resistivity was 18.2 $\text{M}\Omega\text{ cm}$.

The electrochemical oxidation and reduction of the zinc electrode took place in a three-electrode cell, see below. The oxidation was performed in 0.5 M NaOH at -0.95 V vs Ag/AgCl. This corresponds to a potential at which zinc is passivated. The reduction took place in either 0.5 M NaClO₄ at -1.25 V , 0.5 M NaOH at -1.65 V , or 0.1 M LiCl at -1.3 V . All potentials are against the Ag/AgCl reference electrode. These potentials coincide with the reduction of zinc oxide. After the electrochemical surface modification, the sample was quickly rinsed with ethanol to remove residues of the electrolyte and then immediately immersed in the ODT/ethanol (mostly 1 mM, in some cases 20 mM) solution.

The roughness of the samples was investigated with atomic force microscopy. The oxidized zinc samples were seen to be rougher than the reduced zinc samples, as the R_p values for the oxidized samples (highest peak above the mean plane) were about ten times higher than those of the reduced zinc samples.

2.3. Sum Frequency Generation. The laser employed is an Ekspla Nd:YAG picosecond laser (PL2143/20) with an output wavelength of 1064 nm, 24 ps long pulses, and a repetition rate of 20 Hz. It is active/passive mode locked. The laser pumps an optical generator/optical parametric amplifier (OPG/OPA) from Laservision. The pumping energy is around 30 mJ. The visible beam is produced by frequency doubling of the fundamental 1064 nm in a potassium titanyl phosphate (KTP) crystal, subsequently generating a 532 nm output. Part of the 532 nm is used as a pump in the first stage of the OPA/OPG. This stage consists of two angle-tuned KTP crystals. The generated idler (1.2–1.6 μm) from this stage is used in the second step to produce mid-IR frequencies by difference frequency mixing together with a part of the 1064 nm beam.

The energy of the generated IR beam is approximately 300 μJ and the bandwidth is 7 cm^{-1} in the 2800–3100 cm^{-1} region. The IR wavelength was scanned in increments of 1 cm^{-1}/s by four, computer-controlled, dc motors. The beam configuration was that of a copropagating geometry, with the visible and IR beams having incident angles of 55° and 63°, respectively. Both beams were collimated to avoid sample damage. The laser spots had a diameter of about 3 mm at the sample with an energy density of $\sim 4\text{ mJ}/\text{cm}^2$.

The generated sum frequency (SF) beam was passed through a band-pass filter (Omega Optical) to remove residual 532 nm light and then focused into the slits of a monochromator (Jobin Yvon). The dispersed signal was collected by a photomultiplier tube from Hamamatsu (R3788). The signal was averaged by a gated, integrated boxcar (Stanford Research Instruments, SR250) and sent to a Labview program (National Instruments). The IR beam was blocked before each scan (no SFG) to obtain a baseline signal.

A small part of the IR and visible beams was directed into energy meters (Moletron energy meter EPM2000 and J5-09 probes) in order to account for fluctuations in energy to normalize the SFG response. As a reference for the day-to-day

changes in intensities of the SFG signal, a spectrum of clean gold surface was taken before each sample and used for normalization. To ensure that no sample damage occurred by the laser beams, the IR and visible energies were varied individually. The normalized response was seen to be the same for different energies, so it could be concluded that there was no sample damage, as the normalization would fail if the sample was changing during irradiation.

The intensity, I_{SFG} , of the SFG spectra was fitted to a Lorentzian function with Origin software (eq 1). To account for experimental scattering of the data, the instrumental weighting option was used in the error analysis. Here, n is the number

$$I_{\text{SFG}}(\omega_{\text{IR}}) \propto \left| \chi_{\text{NR}}^{(2)} + \sum_n \frac{A_n}{\omega_n - \omega_{\text{IR}} - i\Gamma_n} \right|^2 \quad (1)$$

of vibrational resonances in the spectrum, ω_n is the peak wavenumber of the resonances, A is the amplitude of the vibration, ω_{IR} is the infrared frequency of the light, and Γ_n the damping constant. $\chi_{\text{NR}}^{(2)}$ is the nonresonant background that originates from the substrate, which is complex.

2.4. SFG Microscope. The details of this setup have been described elsewhere.¹⁵ In short, the sum frequency beam was imaged onto a holographic reflective grating by two camera lenses. The microscope collected the intermediate image from the grating by use of a 10 \times objective for magnification and a tube lens for collimation. A Roper CCD camera with a 1024 \times 1024 pixel array was used for detection. Images were acquired by continuously scanning the IR at 0.02 cm^{-1}/s and accumulating 5 000 shots on the camera which provided one image per 5 cm^{-1} . The images were stacked in ImageJ, and integration through the stack produced an SFG spectrum from those pixels in the region-of-interest. The field of view was 1 mm \times 1 mm, and the lateral resolution was 10 μm .

2.5. Electrochemistry. A 1286 Solartron electrochemical interface and a 1255 Solartron frequency analyzer were used in the electrochemistry experiments, which took place in a normal, three-electrode electrochemical cell. The counter electrode consisted of a platinum wire, and the reference electrode was an Ag/AgCl (saturated KCl) electrode. The working electrode was a zinc cylinder, with the polished side touching the surface in a hanging meniscus configuration so that only the polished end of the zinc cylinder was in contact with the solution.

The electrolytes were bubbled with N₂ for at least 30 min prior to the experiment to remove oxygen from the solutions. In the EIS measurement, the sample was at open circuit potential and the frequency range between 1 \times 10⁴ and 0.1 Hz. A 10 mV ac perturbation voltage was applied. A scan rate of 20 mV/s was used during cyclic voltammetry measurements.

2.6. X-ray Photoelectron Spectroscopy. The surface chemical composition was analyzed with XPS by use of a Kratos AXIS HS X-ray photoelectron spectrometer (Kratos Analytical, Manchester, U.K.). XPS spectra were recorded in the fixed analyzer transmission mode with a Mg K α X-ray source operated at 240 W (12 kV/20 mA). The area of analysis was approximately 1 mm². Detailed spectra for O 1s, C 1s, and S 2p were acquired with a pass energy of 80 eV.

2.7. Atomic Force Microscopy. The atomic force microscopy (AFM) measurements were performed in contact mode with a resolver from Quesant Ltd. equipped with the iProbe package supplied by Windsor Scientific Ltd., U.K.

3. Theory

SFG is a nonlinear spectroscopy technique which is inherently surface sensitive. The SFG signal is generated in noncentrosymmetric media which occurs at phase boundaries. Therefore, SFG is able to probe any interface accessible by light.

Two incident beams impinge on the surface, one in the visible (532 nm) and the other in the infrared (IR) region, which overlap in space and time at the interface. The IR frequencies are scanned while the visible (532 nm) is kept constant. The spectrum obtained is a vibrational spectrum.^{16,17} The process is divided into two parts, a resonant IR absorption and a nonresonant Raman scattering. The IR absorption excites the molecule to a higher vibrational state, while an anti-Stokes Raman scattering process occurs simultaneously, emitting a photon in the process, which is the sum of the frequencies of the two incoming beams. The intensity of the sum frequency light depends on the intensity of the incoming beams and the second-order nonlinear susceptibility, $\chi^{(2)}$. L_{SFG} , K_{vis} , and K_{IR} are the Fresnel factors.

$$I_{\text{SFG}} \propto |\chi_{\text{eff}}^{(2)}|^2 I_{\text{IR}} I_{\text{vis}} L_{\text{SFG}} K_{\text{vis}} K_{\text{IR}} \quad (2)$$

The second order nonlinear susceptibility $\chi_{\text{eff}}^{(2)}$ includes the information about the molecules at the surface. It involves a contribution primarily from the substrate, $\chi_{\text{NR}}^{(2)}$, as well as from the resonant part, $\chi_{\text{R}}^{(2)}$, which contains the vibrational resonant contribution.

$$\chi^{(2)} = \chi_{\text{NR}}^{(2)} + \sum_n \chi_{\text{R},n}^{(2)} \quad (3)$$

where n is the number of vibrational resonances.

$$\chi_{\text{R}}^{(2)} = \frac{N}{\epsilon_0} \langle \beta_{\text{R}}^{(2)} \rangle \quad (4)$$

$\chi_{\text{R}}^{(2)}$ depends on N , the number of molecules, the orientational average of $\chi_{\text{R}}^{(2)}$, the hyperpolarisability, and the dielectric permittivity, ϵ_0 . Therefore only molecules with a net orientation are observed in SFG spectroscopy. $\beta_{\text{R}}^{(2)}$ is connected to the IR transition dipole moment and the Raman transition polarizability matrix element.

$$\beta_{\alpha\beta\gamma}^{(2)} = \frac{\alpha_{\alpha\beta} \mu_{\gamma}}{\omega_n - \omega_{\text{IR}} - i\Gamma_n} \quad (5)$$

Here, $\alpha_{\alpha\beta}$ is the Raman polarizability tensor element and μ_{γ} is the IR transition dipole moment. ω_n is the wavenumber of the n th vibrational resonance and ω_{IR} is the frequency of the IR beam, Γ_n is the damping constant, and i is the imaginary unit. On the basis of eq 5, the SFG intensity increases when the IR frequency is close to a vibrational resonance.

Several different polarization combinations of the SFG can be employed to deduce the $\chi^{(2)}$ tensor elements. The polarization combination used herein is PPP (P-polarized sum frequency beam, P-polarized visible beam, and P-polarized IR beam). P-polarized light refers to the light with polarization parallel to the plane of incidence as opposed to S-polarized light, which is light polarized perpendicular to the plane of incidence. The SSP spectra for ODT on zinc were much weaker than the PPP spectra and gave no additional information.

4. Results

4.1. Sum Frequency Generation. The vibrational modes observed in the CH stretching region (2800–3000 cm^{-1}) for

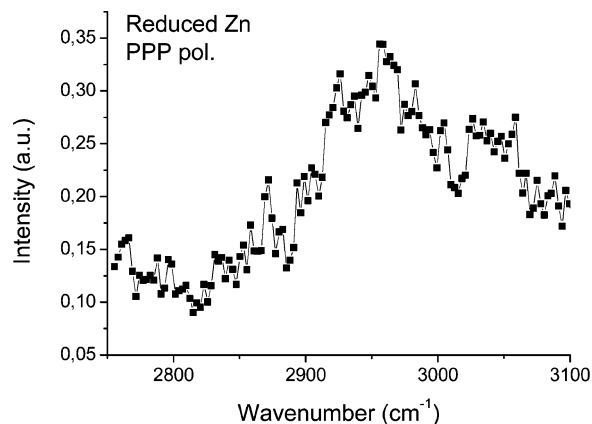


Figure 1. Zn reduced in 0.5 M NaClO_4 at -1.25 V for 30 min. SFG collected in N_2 atmosphere.

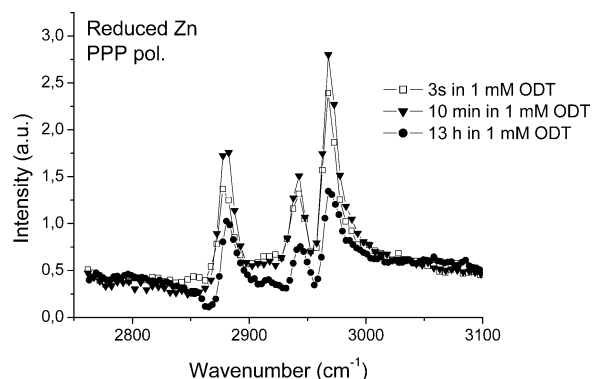


Figure 2. Zn reduced in 0.5 M NaClO_4 at -1.25 V for 30 min before immersion in ODT solution. PPP polarization SFG spectra for different immersion times in 1 mM ODT/ethanol solution. Spectra collected in air.

long hydrocarbon chains are different types of CH_3 and CH_2 vibrations. The presence of CH_2 peaks indicates that the chains contain gauche defects.^{16,18} If the chains are in an all-trans configuration, pairs of the methylene groups are related by the inversion symmetry. Deviations from the all-trans configuration produce a broken symmetry and therefore generate an SFG signal.

The spectrum of bare zinc in Figure 1, prepared by reduction in 0.5 M NaClO_4 at -1.25 V for 30 min, shows signs of weak resonances in the CH stretching region (2800–3000 cm^{-1}), which correspond to contamination from various carbon-containing species. The spectrum was taken with the sample in a dry N_2 atmosphere to minimize contamination. Hence, the spectrum for the bare zinc surface corresponds to the condition of the sample as it is immersed in the thiol solution.

4.1.1. Reduced Zinc in 1 mM ODT Solution. In Figure 2, the PPP polarized spectrum for reduced zinc immersed in 1 mM ODT/ethanol solution is seen. The peaks corresponding to CH_2 stretching vibrations are the symmetric stretch at 2850 cm^{-1} and the asymmetric stretch at 2915 cm^{-1} . The CH_3 vibrational modes consist of the symmetric stretch, the Fermi resonance, and the asymmetric stretch at 2880, 2940, and 2970 cm^{-1} , respectively.¹⁹ In Figure 2 for the reduced zinc immersed for 3 s in a 1 mM ODT/ethanol solution, an ordered adsorbate is rapidly formed on the surface. This observation is based on the fact that the methylene vibrations are weak; the spectrum is dominated by the three methyl vibrations. Note that the intensity scale is different compared to that of the bare zinc in Figure 1, as the intensity of the peaks are about 10 times stronger in the case of the samples immersed in ODT.

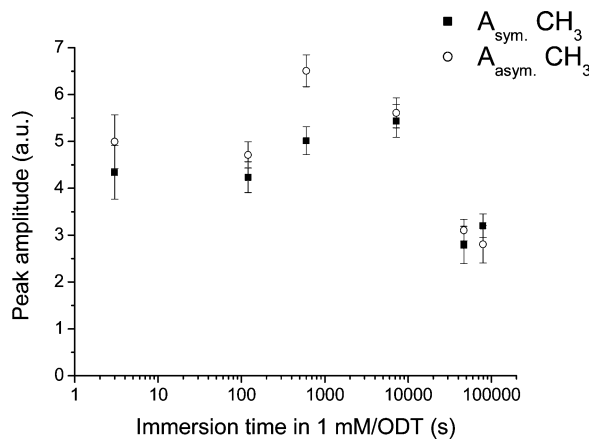


Figure 3. Reduced zinc immersed in 1 mM ODT/ethanol solution. Amplitudes of the fitted CH₃ vibrations from PPP polarized spectra.

After 10 min immersion time, the PPP polarization spectrum is similar to the corresponding ODT spectra for gold^{20,21} in the sense that the only peaks observed are the three strong CH₃ resonances.

The CH₂ peaks increase slightly in intensity for longer immersion times, as seen in Figure 2.

In Figure 3, amplitudes of the methyl vibrations at 2880 and 2970 cm⁻¹ are plotted. These were obtained from the fittings using the Lorentzian function (eq 1). The ratio of the fitted amplitudes of the symmetric and asymmetric CH₃ is used to estimate orientational changes at the surface.^{22–24} A plot of the ratio of the symmetric and asymmetric amplitudes versus the tilt angle from the surface normal to the C₃ axis can be constructed from the theoretical calculations, assuming that all molecules have exactly the same orientation, i.e., a delta distribution of the angles. When the experimental amplitude ratio is compared with this plot, the tilt angle can be obtained.

Figure 4A shows that the ratio of the fitted amplitudes of the symmetric and asymmetric CH₃ stretches stays the same, within the experimental error, throughout the entire immersion time range. The formulas used for the orientation calculations were based on the ones presented by Wang et al.²⁴ with the bond polarizability model.^{25,26} The Fresnel factors were calculated by use of the equations presented by Shen et al.,²² and the refractive indices used were 0.53 + 3.4*i* for the SF beam (460 nm),²⁷ 0.85 + 4.1*i* for the visible beam,²⁷ and 1.13 + 12.6*i* for the IR beam.²⁸ The value used for the interfacial refractive index, *n'*, was 1.4648.²⁹ Assignment of this value is not clear, so plots for different values have been generated to investigate the sensitivity of this parameter. The value employed for the bond polarization derivative ratio *r* was 0.026. The result plotted in Figure 5 gives a tilt angle between 39° and 65°, taking both experimental error and different *n'* values into account. This value is only an estimate of the orientation and most importantly shows that the experimental error does not have a great effect on the tilt angle.

In Figure 4B, the fitted SFG amplitudes of the CH₃ peaks at 2880 and 2970 cm⁻¹ have been normalized against the number of molecules, as obtained, and discussed in a later section. Since it was concluded in Figure 4A that there are no orientational changes over prolonged immersion times, within the experimental error, the fitted amplitudes depend on the distribution of orientations of the CH₃ group. The averaging in eq 4 is related to the distribution of the tilt angles of the molecule. When the distribution is narrow, the signal is increased compared to that when it is broad.³⁰ The drop in normalized amplitude that is seen in Figure 4B is then interpreted as a lowering of the

conformational order of the ODT adsorbed on the reduced zinc surface when immersed for longer times in the 1 mM ODT solution. The normalized amplitude of the symmetric CH₃ drops by a factor of 6 during the first 100 s and another factor of 3 between 100 and 10⁵ s immersion.

4.1.2. Oxidized Zinc. The spectrum of the oxidized zinc in Figure 6 for 3 s immersion time depicts an adsorbate with many defects, as the CH₂ vibrations at 2915 and 2940 cm⁻¹ peaks are strong. When compared to the corresponding immersion time for ODT on reduced zinc (Figure 2), it is clear that it takes longer time to form an ordered ODT layer on oxidized zinc than on reduced zinc, as judged from the weaker CH₂ features in Figure 2 than those in Figure 6. In the case of oxidized zinc, it takes about 5 min before a highly ordered adsorbate is formed (Figure 6). For immersion times longer than 2 h, there are no further changes in the PPP polarized spectra (Figure 6). For the oxidized zinc, the plot for the fitted amplitude ratios of the symmetric and asymmetric stretches shows that the tilt angle of the ODT changes with immersion time, making it difficult to investigate if the adsorbates become more or less ordered, as in the case of reduced zinc. On comparison with the PPP spectra of reduced zinc for 24 h immersion time in 1 and 20 mM ODT solutions (Figure 7), it is apparent that the differences between the two are negligible. The same holds true for oxidized zinc in Figure 8.

The nonresonant background of the zinc affects the shape of the spectrum by interfering with the resonant signal. Equation 2 can be written as

$$I_{\text{SFG}} \propto |\chi_{\text{NR}}^{(2)} + \chi_{\text{R}}^{(2)}|^2 = |\chi_{\text{NR}}^{(2)}e^{i\varphi} + \chi_{\text{R}}^{(2)}e^{i\delta}|^2 \quad (6)$$

Here φ and δ are the phases of the nonresonant and resonant susceptibilities, respectively. The phase of the nonresonant background is 120° for reduced zinc at 3 s immersion time. It increases with immersion time, and at 24 h it is 158°. For the oxidized zinc, the nonresonant phase has a similar trend. It increases from 120° at 3 s to 174° at 24 h immersion time. This change in phase results in a change in the shape of the SFG spectra, as seen in Figures 2 and 6. For comparison, the nonresonant phase for ODT on zinc is different than those on gold (90°) and silver (-45°).¹⁶

To summarize, the ODT forms an ordered adsorbate within seconds on reduced zinc and somewhat slower on oxidized zinc. An increase in the ODT concentration does not result in any visible changes in the PPP spectra for longer immersion times.

4.2. X-ray Photoelectron Spectroscopy. XPS was used to provide complementary information on the bonding between adsorbed ODT on reduced and oxidized zinc surfaces. The binding energy for the S 2p peak of both the reduced and the oxidized zinc is located at 163 eV (Figure 9). This corresponds to a zinc–sulfur bond³¹ and is in line with the results of Mekhalif et al.³² This binding energy is well separated from sulfur bonded to oxygen, which has binding energies in the range from 165.5 to 169 eV.³³

For immersion times up to 24 h and ODT concentrations of 1 and 20 mM, the peak position of the S 2p peak does not change. This indicates that no oxygen–sulfur bonds are created even at longer immersion times and higher ODT concentrations. Oxidized carbon species, representative of organic contaminants with binding energies higher than 285 eV, are present on both reduced and oxidized zinc (not shown). However, when the ODT is adsorbed, these peaks disappear. This manifests the known ability of the thiols to displace weakly adsorbed species upon adsorption.⁵ The peak corresponding to aliphatic carbon at 285 eV remains, as it represents the ODT.

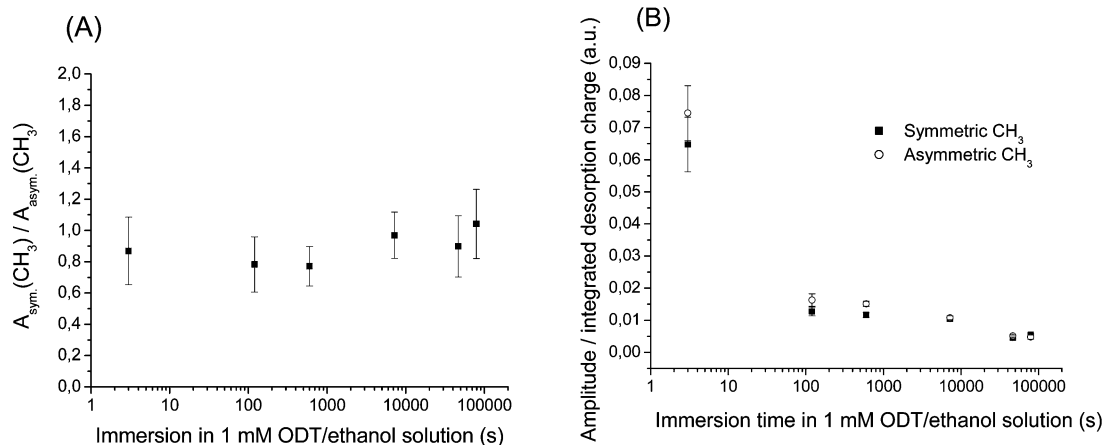


Figure 4. (A) Ratio of fitted amplitudes for reduced zinc immersed in 1 mM ODT/ethanol solution. The amplitudes are for the symmetric CH_3 and asymmetric CH_3 vibrations. (B) The amplitudes of the CH_3 vibrations in Figure 4A have been divided by the integrated charge.

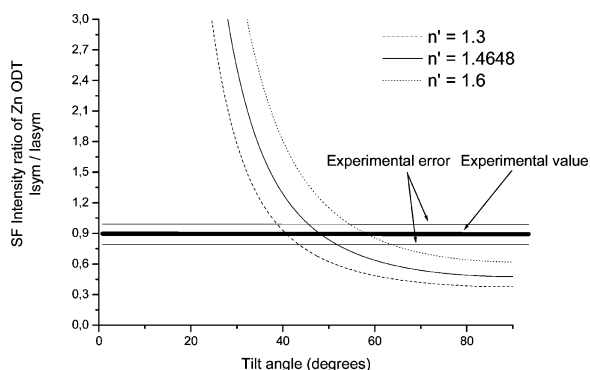


Figure 5. Simulation of the SFG signal for the intensity ratio between the symmetric CH_3 and the asymmetric CH_3 stretches of ODT on zinc for different values of n' to determine the tilt angle.

4.3. Electrochemistry. 4.3.1. Cyclic Voltammetry. It has been shown that thiols on gold^{34–36} and zinc⁸ undergo reductive desorption in a one-electron process. This allows the number density of the adsorbed thiols to be calculated from the integrated charge of the reductive desorption peak. The double-layer charge contributes to the total charge, so it has to be subtracted before a calculation of the number density is possible. The double-layer charge calculated by Zhang et al.⁸ was $6.4 \mu\text{C}/\text{cm}^2$.

The cyclic voltammograms in Figure 10 display the formation of zinc oxide at around -1.15 V and reduction of the oxidized species at -1.25 V .³⁷ The sharp increase in current at -1.6 V is the onset of hydrogen evolution. The peak of the ODT reductive desorption is located near -1.5 V for 1 and 22 h of immersion times. Note that for reduced zinc after 3 s immersion time in 1 mM ODT the peak for reduction of oxide is present along with the reductive peak of the ODT at -1.5 V . This means that the surface after 3 s immersion consists of both zinc oxide and adsorbed ODT. The integrated charge, q , of the ODT reductive peak is calculated from eq 7

$$q = \int_{E_1}^{E_2} \frac{|i|}{\nu} dE \quad (7)$$

where q is the charge, E is the potential range, i is the current, and ν is the scan rate. After 1 h immersion time, the integrated charge is around $650 \mu\text{C}/\text{cm}^2$ and does not increase with prolonged immersion time. When dividing the integrated charge with the charge of the electron, since it is a one-electron process, the density for adsorbed ODT obtained is 4.1×10^{15} molecules/ cm^2 or 6.7×10^{-9} mol/ cm^2 (Figure 11). This value is about 10

times higher than the reported number for gold, 4.3×10^{14} molecules/ cm^2 .^{35,36} One reason for this discrepancy is the fact that the density for adsorbed gold is from smooth single crystalline gold, whereas a polycrystalline polished zinc substrate was used here, making the surface area higher. The corresponding density number after 1 h immersion time for zinc oxidized in 0.5 M NaOH at -0.95 V to a charge of $300 \mu\text{C}/\text{cm}^2$ is close to that of reduced zinc, 6.7×10^{-9} mol/ cm^2 . The plots in Figure 11 show that the oxidized and reduced zinc adsorb the ODT molecules at similar rates.

Peak position of the reductive desorption gives conformational information of the thiols on the zinc surface. A more negative potential for the reductive desorption means that the film is associated with more well-ordered, long-chain thiols.^{35,36} The peak position for the ODT desorption for 3 s immersion time is located at a more negative potential than those for longer immersion times (Figure 10). This suggests that the short immersion time compared to the longer time creates a more well-ordered film, in agreement with the SFG results.

4.3.2. Electrical Impedance Spectroscopy. 4.3.2.1. The Substrates before Modification with ODT. The Nyquist plot in Figure 12 of the reduced and oxidized samples show that the oxidized zinc forms a more protective film than the reduced zinc, as judged from the higher impedance and the appearance of a semicircle for the oxidized zinc.³⁸ It is not clear if all the zinc oxide is removed during the reduction, but the surface after reduction is more active than the surface before, since the open circuit potential has decreased.

EIS data for self-assembled monolayers of thiols on gold have previously been fitted with a constant phase element (CPE) in parallel with a resistor.^{8,39} The CPE accounts for defects in the film, such as step edges, grain boundaries, and point defects. In other cases, a capacitor in series with a resistor corresponding to the solution resistance has been used.⁴⁰ This corresponds to a more ideal response, in which the adsorbate forms a perfect insulating monolayer, making its electrical response identical to that of a pure capacitor.

4.3.2.2. Reduced Zinc Immersed in 1 and 20 mM ODT/Ethanol Solutions. For short immersion times, it is clear that the ODT solution has not yet formed a protective layer, as seen in the plot for 3 s immersion time in Figure 13. The simple CPE circuit does not yield a good fit. The impedance is higher compared to the bare reduced sample. After 1 h, the protective ability of the adsorbate has increased significantly. A good fit for a simple circuit with the CPE in parallel with a resistor is still not possible. However, the electrochemical impedance

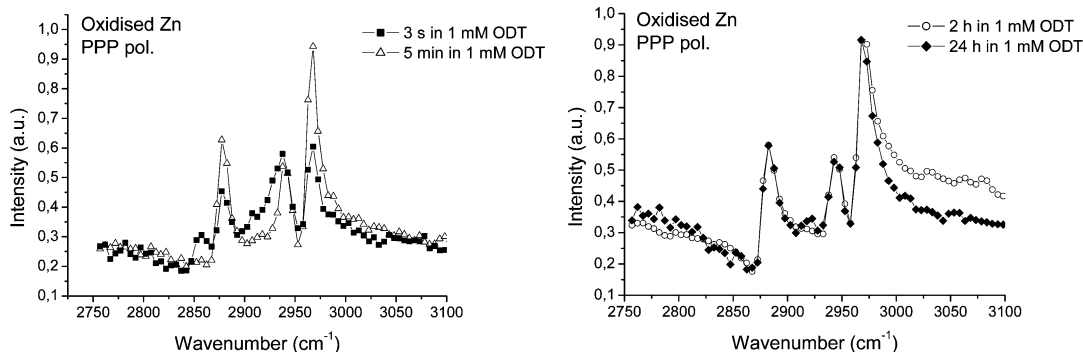


Figure 6. Zn oxidized in 0.5 M NaOH at -0.95 V to a total charge of 300 mC/cm^2 . PPP polarization SFG spectra for different immersion times in 1 mM ODT/ethanol solution. Spectra collected in air.

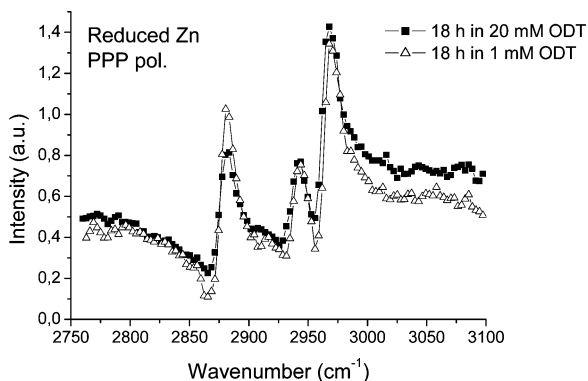


Figure 7. Zn reduced in 0.5 M NaClO_4 at -1.25 V for 30 min before immersion in ODT solution. PPP polarized SFG spectra after 18 h in 1 mM and 20 mM ODT concentrations, respectively.

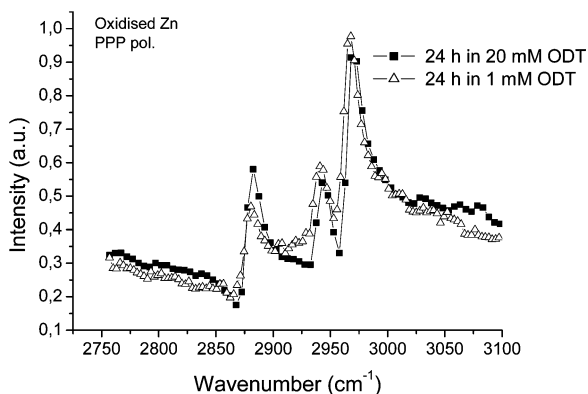


Figure 8. Zn oxidized 300 mC/cm^2 in 0.5 M NaOH before immersion in ODT solution. PPP polarized SFG spectra after 24 h in 1 mM and 20 mM ODT concentrations, respectively.

behavior is better fitted to this circuit than for shorter immersion times. The increased protection is also manifested in the open circuit potential as it increases from -1.12 to -1.04 V.

After 24 h in 1 mM ODT solution, the protective quality of the film has decreased. The impedance is much lower compared to that of the 1 h immersion time. As judged from the phase angle close to 45° at high frequencies (Figure 13), the system exhibits diffusion-limited behavior at low frequencies, presumably the diffusion of ions across the electrochemical interface.³⁸ The phase angle is defined as the angle between the real and imaginary impedance. This leads to the conclusion that the surface has now degraded and ions are able to diffuse through the adsorbate. Note, from Figure 11, that the decrease in impedance does not originate from desorption of the ODT adsorbates. Figure 11 shows that the amount of adsorbed surface species levels off at higher immersion times, while the imped-

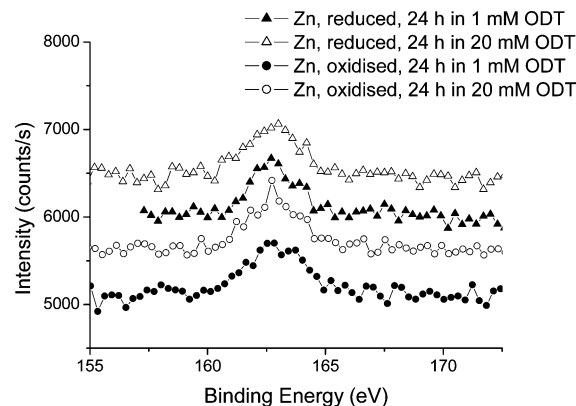


Figure 9. XPS spectra of Zn oxidized in 0.5 M NaOH at -0.95 V to a total charge of 300 mC/cm^2 and of Zn reduced in 0.5 M NaClO_4 at -1.25 V for 30 min and then immersed in 1 or 20 mM ODT for 24 h. Closed triangles, reduced Zn in 1 mM ODT; open triangles, reduced Zn in 20 mM ODT; closed circles, oxidized Zn in 1 mM ODT; open circles, oxidized Zn in 20 mM ODT.

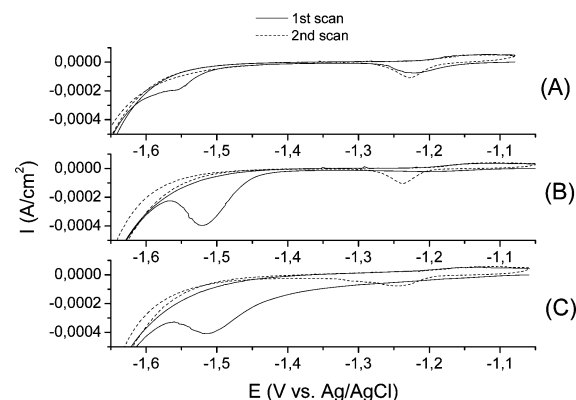


Figure 10. Cyclic voltammograms of zinc reduced in 0.5 M NaClO_4 at -1.25 V for 30 min before immersion in ODT: (A) Immersed in 1 mM ODT for 3 s. (B) Immersed in 1 mM ODT for 1 h. (C) Immersed in 1 mM ODT for 22 h. Scan rate: 20 mV/s.

ance (protective ability) decreases as seen in Figure 13. When immersed in 20 mM ODT/ethanol solution for 24 h, the impedance was much higher than that obtained for 1 mM solution and also the fit to a CPE circuit was better.

To determine if oxygen in the ethanol solution could be the cause of the decrease in the corrosion protection of the adsorbate, a deaerated solution of ethanol was used, but the result was similar to that of the aerated solution.

4.3.2.3. Oxidized Zinc Immersed in 1 and 20 mM ODT/Ethanol Solutions. The impedance for the oxidized zinc resembles that of the reduced zinc, as seen in Figure 14. As before, no simple equivalent circuit is able to fit the spectra.

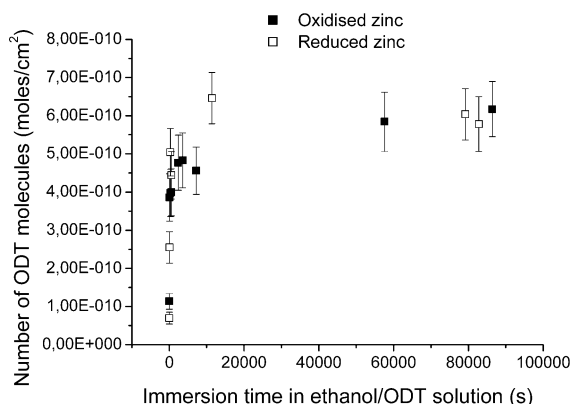


Figure 11. Densities of adsorbed ODT for reduced and oxidized zinc after immersion in 1 mM ODT.

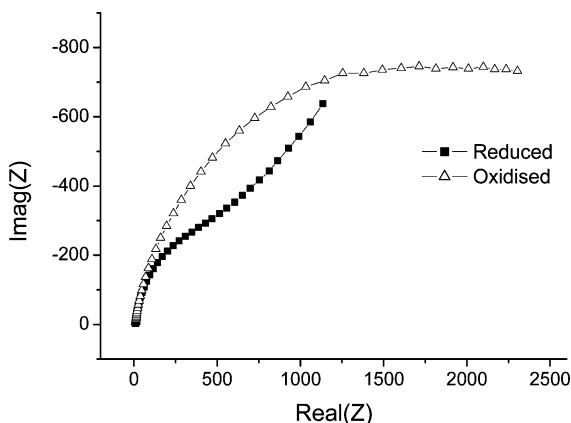


Figure 12. Nyquist plot of Zn reduced in 0.5 M NaClO₄ at -1.25 V and of Zn oxidized in 0.5 M NaOH at -0.95 V. Both impedance spectra were taken in 0.5 M NaClO₄ and 5 min after reduction or oxidation.

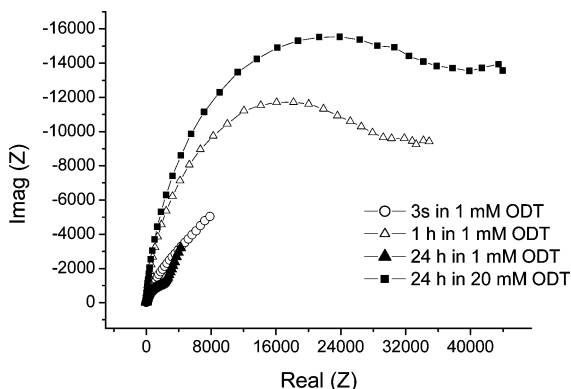


Figure 13. Nyquist plots of zinc reduced in 0.5 M NaClO₄ at -1.25 V for 30 min before immersion in ODT. Impedance spectra taken in 0.5 M NaClO₄.

For up to 2 h of immersion in the ODT solution, the impedance of the film is increasing. The increase in open circuit potential by 100 mV from 1 min to 2 h immersion time also supports the fact that the surface film becomes more protective.

The increased concentration of ODT in the solution again increases the quality of the film (Figure 14). The impedance is clearly higher. Compared to the reduced zinc, the improvement is smaller when the concentration is increased from 1 to 20 mM.

A direct comparison between the values of the resistance and the desorption charge between the reduced and oxidized zinc is not possible due to the difference in surface area. When all the zinc has been oxidized, a rougher surface is obtained with

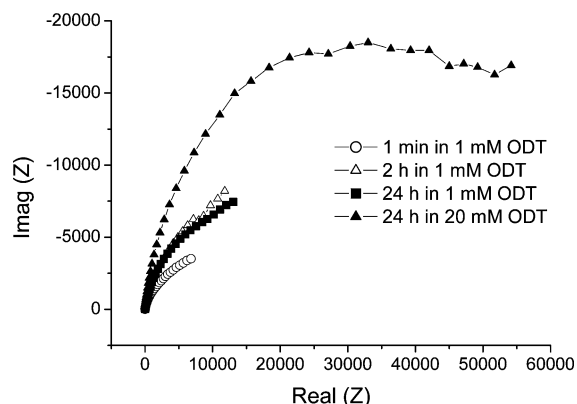


Figure 14. Nyquist plots for zinc oxidized in 0.5 M NaOH with 300 mC/cm² charge before immersion in ODT. Impedance measured in 0.5 M NaClO₄.

a higher surface area that influences the impedance value. Presumably, the number of molecules on the surface is also affected, as more sites are potentially available.

In all, the ODT adsorbed on reduced and oxidized zinc is seen to form a protective barrier. However, the film behavior is complicated, and a simple equivalent circuit cannot match the impedance response. Increasing the ODT concentration improves the corrosion protection.

4.4. Sum Frequency Generation Imaging. SFG imaging microscopy has been shown to give lateral information of surface species in the case of CO adsorbed on platinum,⁴¹ in micro contact printing,¹⁵ and ODT adsorbed on gold and mild steel.³⁰ The image obtained by the SFG microscope in Figure 15 suggests that the surface is indeed heterogeneous. There are areas with a clear spectrum of the CH₃ vibrations, corresponding to an ordered ODT adsorbate (spectra D and E in Figure 15), regions which shows many similarities to a spectra with CH₃ peaks (spectra B and C in Figure 15), and areas with little resemblance to adsorbed ODT (spectra F and G in Figure 15). Even though significantly different domains are seen on the surface, the spectrum representative of the overall image indicates a well-ordered ODT adsorbate (Figure 15A). The shape of the ODT spectrum in Figure 15A is different than the ones in Figures 2 and 6. This can be explained by the use of a 1064 nm as the “visible” probe in the SFG imaging as opposed to 532 nm in the other SFG experiments. The change in wavelength of this probe affects the nonresonant background, which in turn has an impact on the spectral shape. The resulting main conclusion from the SFG imaging is that the surface is chemically heterogeneous with domains of ordered ODT and areas of oxide and/or less ordered ODT.

5. Discussion

The most common concentration used for forming self-assembled monolayers of thiols on gold is 1 mM in an ethanol solution. For gold, the immersion time suggested is around 24 h.¹ Since zinc is an active metal, it is more sensitive than gold to immersion time, concentration of thiols, and choice of the solvent. The first two of these parameters will be discussed later in this section. It has been proposed that a higher concentration of the thiol improves the contact angle⁴ in the case of copper and leads to a higher coverage⁴² in the case of zinc. The ODT forms an ordered self-assembled adsorbate on both oxidized and reduced zinc.⁸

Three steps in the adsorption of ODT on reduced zinc can be distinguished, as schematically depicted in Figure 16. The first step is a very fast initial step where the ODT forms ordered,

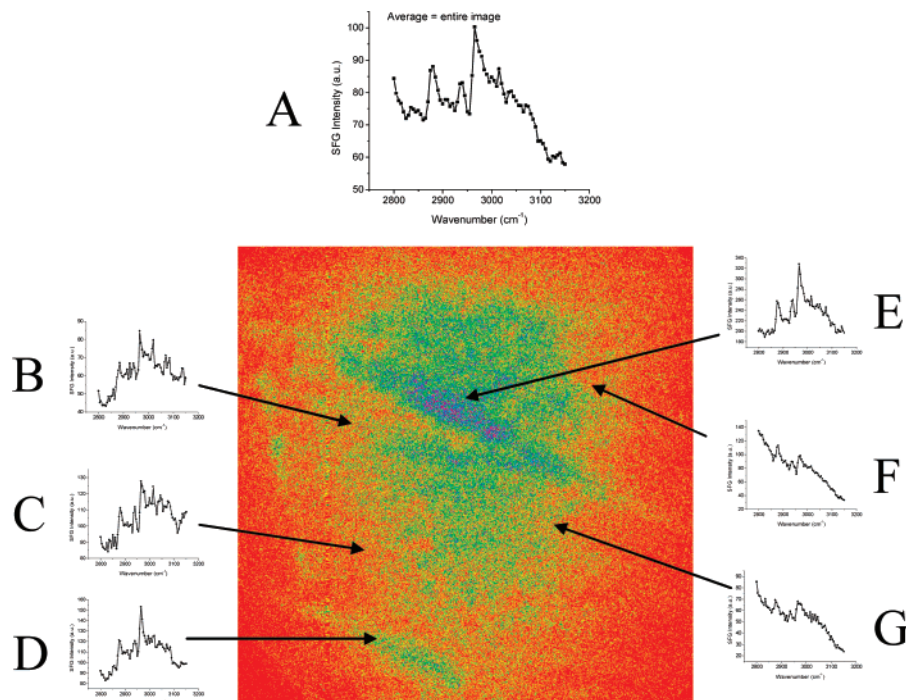


Figure 15. SFG image of Zn reduced in 0.5 M NaOH and immersed in 1 mM ODT for 2 h. Size of the image is 1 mm \times 1 mm. (A) Average SFG spectrum over the entire image. (B–G) SFG spectra of selected regions on the image.

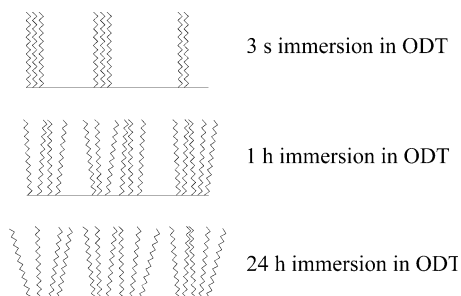


Figure 16. Schematic view of ODT adsorbed on reduced zinc at different immersion times in 1 mM ODT. The ratio between the regions covered and uncovered by the ODT should not be taken as the absolute values; the figure is only for schematic purposes. The tilt angle from the surface normal to the hydrocarbon chain has previously been suggested to be 0°.⁸

highly oriented, regions (3 s immersion, Figure 2) which increase the corrosion protection properties (Figure 13). It can be seen in Figure 11 that the number of adsorbed molecules is far from saturation, so ODT is not yet covering the whole surface. The next step is from 3 s to 1 h immersion time. After 1 h, the number of ODT molecules on the reduced zinc surface reaches saturation, as seen with CV in Figure 11. The adsorbate becomes less ordered compared to that of 3 s immersion time (Figure 4B) during this time period. The EIS shows that the corrosion protection increases on going from 3 s to 1 h immersion time, as seen in the increase in impedance. Hence, the improved corrosion protection observed on going from 3 s to 1 h immersion time in 1 mM ODT is due to less ordered ODT adsorbed on the reduced zinc. The last step is from 1 to 24 h immersion time. The SFG shows that the ODT now contains some defects, as judged from the appearance of CH₂ peaks in Figure 2 after 13 h, and also continues to become less ordered (Figure 4B). This is accompanied by a drop in the impedance, which represents the corrosion protective ability of the adsorbate, between 1 and 24 h immersion time in 1 mM ODT, as seen in Figure 13. The number of adsorbed ODT molecules stays basically the same between 1 and 24 h immersion time (Figure

11). Hence, the decrease in corrosion protection can be related to defects and lesser ordering of the ODT adsorbate. Now, a clear difference can be seen when comparing with thiols adsorbed onto gold. For that system, a longer immersion time continuously improves the ordering of the thiol.¹ This is not the case for ODT adsorbed on zinc, where immersion times longer than 1 h decrease both ordering and protective ability of the adsorbed ODT. These results do not agree completely with those of Nogues et al.,⁹ where long immersion times are seen to improve ordering of the adsorbate. The fact that a different preparation method was used, the sample was polished in thiol before immersion in a neat thiol solution for 48 h, could affect the results. The preparation parameters have been seen to strongly influence the resulting ODT adsorbate. The use of pure thiol liquid by Nogues et al., rather than as a solution in ethanol, may possibly have avoided the harmful effect of ethanol, as will be discussed later. Their results from contact angle measurements show similarities to the CV desorption data in Figure 11, a rapid absorption of the thiol molecules followed by flattening of the curve when adsorption of the ODT slows down.

The results show that the system consisting of the ODT adsorbed on reduced zinc is more complicated than the corresponding one for gold and lead to a discussion of the homogeneity of the surface.

From the EIS data, presented as Nyquist plots (Figure 13), it is clear that no equivalent circuit describing a perfectly insulating adsorbate can fit this spectrum. A more suitable model is an electrical circuit consisting of a constant phase element (CPE) in parallel with a resistor as a way to account for imperfections of the adsorbate. However, this model is still not adequate. Imperfections on the surface causing a nonhomogeneous adsorbate are also observed in the SFG microscope image in Figure 15, where clearly different regions on the surface are present. Hence, both the EIS and the SFG imaging results suggest a heterogeneous surface, and no simple model of the surface is possible. Some regions consist of ordered ODT molecules, and some consist of either disordered ODT or no

adsorbed ODT species at all but only surface oxides. This again is different from what is seen for thiols adsorbed on gold. Although domains with less ordering for butanethiol adsorbed onto Au(111) studied with STM⁴⁴ were observed, these regions are much smaller than the ones in Figure 15.

XPS measurements were performed to reveal the nature of the bonding between ODT and the reduced zinc surface. Zinc modified with thiols has been studied earlier with XPS.³² In these studies, zinc, which had been reduced or left in air to form an oxide for 3 min, was immersed in *n*-dodecanethiol for 12 h before being studied by XPS. A binding energy of 162.8 eV for the S 2p peak, Figure 9, concludes that the ODT binds to the reduced zinc surface by forming a Zn–S bond. The same observation was seen for oxidized zinc.

Also in the case of ODT adsorbed on oxidized zinc, three steps in the adsorption process can be identified, as discussed next. The first step in the adsorption process, up to 5 min immersion time, is different than that for the reduced zinc. On the basis of the appearance of the CH₂ peaks in the SFG spectra (Figure 6, left), it takes around 5 min to form highly ordered regions of ODT on oxidized zinc compared to 3 s for reduced zinc. One explanation for this is the surface is rougher when oxidized, making it less likely for the ODT to form ordered regions. The roughness decreases the interaction between the hydrocarbon chains of the ODT, as the interfacial area between the molecules is smaller for a rough surface than for a perfectly flat one. The consequence is that the van der Waals forces between the molecules are reduced. Another reason for this slower adsorption time is that the ODT will have to desorb the oxide in order to gain access to the zinc atoms, to which it adsorbs (Figure 9). The second step is from 5 min to 2 h immersion time. During this period, the corrosion protection increases (Figure 14) and the number of adsorbed molecules reaches saturation, as seen in Figure 11. Hence, the second step in the adsorption is similar to that of reduced zinc, with an improved corrosion protection ability. It could originate from low-ordered regions of adsorbed ODT. As noted earlier, a similar detailed analysis concerning the ordering could not be performed. Nevertheless, it is possible that there is a decrease in the ordering between 5 min and 2 h immersion times. The intensities of the peaks in the SFG spectra in Figure 6 for 5 min and 2 h immersion times are similar and, simultaneously, the number of adsorbed ODT for 5 min immersion time is much higher than that of the 2 h immersion time, as seen in Figure 11. This implies, according to eq 4, that the distribution of angles for the ODT has broadened between 5 min and 2 h immersion times. The third step is from 2 to 24 h immersion times in 1 mM ODT solution. Figure 14 exhibits similar impedance spectra for 2 and 24 h immersion times, showing that longer immersion times do not significantly degrade the protective ability of the adsorbed film. In the SFG spectra in Figure 6, it is evident that very little happens in terms of ordering of the ODT. The density of adsorbed ODT does not change between 2 and 24 h immersion times. This adsorption process is different than that for reduced zinc, where the corrosion protective ability of the adsorbate decreases for longer immersion times. The difference may be related to the fact that the oxidized surface is more passive from the beginning thus making it less susceptible to degrade when immersed in the ODT/ethanol solution. Complementary XPS data, Figure 9, again show that the ODT binds to the oxidized zinc surface by forming a Zn–S bond, similar to ODT adsorption on reduced zinc. As in the case with reduced zinc, when the ODT adsorbed on oxidized zinc is compared to the system of thiols adsorbed on gold, it is evident that there is

a difference between the two. The ODT on oxidized zinc is not able to form defect-free films and also does not improve its corrosion protection with longer immersion times (up to 24 h).

Higher concentration (20 mM) of ODT in solution (compared to 1 mM) increases the impedance (protective ability) of both the reduced and the oxidized zinc. For longer immersion times, the highest improvement in the impedance is seen for the reduced zinc. The Nyquist plot in Figure 13 shows a far better protected surface at higher concentration. This leads to the possibility that there are competing surface processes during the adsorption of ODT on reduced zinc, one being the adsorption of ODT itself and the other a surface related process that prevents the adsorption, deteriorates adsorbed ODT, or degrades the surface. Interaction between ethanol and the zinc surface is a possible reason for this degrading reaction, as it has been suggested that ethanol is not an appropriate solvent for self-assembling of thiol.⁴² This confirms the results of Mekhalif et al.,³² wherein they suggested that a higher thiol concentration is beneficial for the quality of the films formed on zinc and zinc oxide. Also, Ron et al.⁴ concluded that for copper oxide a higher thiol concentration was found to promote the formation of high quality films.

On comparison of SFG spectra in Figures 7 and 8 for longer immersion times, no noticeable difference is observed between 1 and 20 mM ODT concentrations. Hence, the improvements in impedance with increased ODT concentration are not related to the molecular arrangements of adsorbed ODT, as deduced by SFG, and therefore must be related to the surface regions to which the SFG is insensitive. The XPS spectra in Figure 9 also show that for 20 mM ODT concentration the adsorbate forms a Zn–S bond.

The overall conclusion is that the surface is divided into different domains: some with highly ordered ODT (as seen with SFG) and some of less protective nature. The latter may consist of completely disordered or highly defective ODT, some other species adsorbed on the zinc surface, or a combination of the two. This is manifested in the SFG microscopic image (Figure 15).

The deviating observations deduced from SFG and EIS reflect the fact that the techniques probe different surface constituents. SFG only detects ordered molecules and is insensitive to regions with completely disordered adsorbates. EIS, on the other hand, probes the electrical response of the whole interfacial region between the solid and the solution, which makes it difficult to model a surface characterized by interfacial areas with very different properties. The combination of several complementary techniques, such as EIS, SFG, and XPS, has demonstrated that a more comprehensive picture can be obtained from the studied ODT–zinc system.

6. Conclusions

ODT adsorbs on the reduced and oxidized zinc surfaces through Zn–S bonds. It is seen that the ODT adsorbs within 3 s on reduced zinc but becomes less ordered with prolonged immersion time. This less ordered film still contributes to an increased corrosion protection until the ODT molecules saturate the surface. An immersion time of about 1 h in the 1 mM ODT/ethanol solution is optimum to form a corrosion resistant adsorbate on reduced zinc, whereas a longer immersion time (24 h) leads to an adsorbate film with lesser molecular ordering and reduced corrosion protection properties. On oxidized zinc, the adsorption process is slower, and only after 5 min immersion time an ordered film is formed. Lower ordered ODT contributes to an increased corrosion protection until the number of ODT

molecules reaches the saturation value. No decrease in corrosion protection with longer immersion times is observed, most likely due to a more passivated zinc surface in areas between adsorbed ODT domains. The adsorbate is heterogeneous and consists of more ordered domains interrupted by less ordered domains or uncovered areas.

This surface deterioration of ODT adsorbed on reduced zinc could be avoided by increasing the concentration to 20 mM, suggesting that there are competing reactions alongside the adsorption and organization of the ODT adsorbate.

The adsorbate formed by ODT on reduced and oxidized zinc is heterogeneous and becomes less ordered when immersed for longer times in 1 mM ODT, a behavior that is distinctly different from that on gold. The number of ODT molecules on the oxidized and reduced zinc surfaces reaches saturation at around 6.7×10^{-9} mol/cm².

Acknowledgment. The Swedish Research Council (VR), Champion Technologies (Houston), and National Science Foundation (NSF) under Grant No. 0650779 are gratefully acknowledged for the financial support. We thank Associate Professor Inger Odnevall Wallinder (Division of Corrosion Science, KTH) for performing the XPS measurements and Ali Davoodi, M.Sc. (Division of Corrosion Science, KTH) for performing the AFM measurements.

References and Notes

- Bain, C. D.; Troughton, E. B.; Tao, Y.-T.; Evall, J.; Whitesides, G. M.; Nuzzo, R. G. *J. Am. Chem. Soc.* **1989**, *111*, 321.
- Yan, C.; Zharnikov, M.; Götzhäuser, A.; Grunze, M. *Langmuir* **2000**, *16*, 6208.
- Keller, H.; Simak, P.; Schrepp, W.; Dembowski, J. *Thin Solid Films* **1994**, *244*, 799.
- Ron, H.; Cohen, H.; Matlis, S.; Rappaport, M.; Rubinstien, I. *J. Phys. Chem. B* **1998**, *102*, 9861.
- Himmelhaus, M.; Gauss, I.; Buck, M.; Eisert, F.; Woll, C.; Grunze, J. M. *Electron Spectros. Relat. Phenom.* **1998**, *92*, 139.
- Volmer-Uebing, M.; Stratmann, M.; *Appl. Surf. Sci.* **1992**, *55*, 19.
- Zhang, H. P.; Romero, C.; Baldelli, S. *J. Phys. Chem. B* **2005**, *109*, 15520.
- Zhang, H. P.; Baldelli, S. *J. Phys. Chem. B* **2006**, *110*, 24062.
- Nogues, C.; Lang, P. *Langmuir* **2007**, *23*, 8385–8391.
- Halevi, B.; Vohs, J. M. *Catal. Lett.* **111** (No. 1, 2), **2006**.
- Dvorak, J.; Jirsak, T.; Rodriguez, J. A. *Surf. Sci.* **2001**, *479*, 155.
- Halevi, B.; Vohs, J. M. *J. Phys. Chem. B* **2005**, *109*, 23976.
- Pesika, N. S.; Hu, Z.; Stebe, K. J.; Searson, P. C. *J. Phys. Chem. B* **2003**, *106*, 6985.
- Wong, E. M.; Hoertz, P. G.; Liang, C. L.; Shi, B.-M.; Meyer, G. J.; Searson, P. C. *Langmuir* **2001**, *17*, 8362.
- Cimatu, K.; Baldelli, S. *J. Phys. Chem. B* **2006**, *110*, 1807.
- Bain, C. D. *J. Chem. Soc., Faraday Trans.* **1995**, *91*, 1281.
- Shen, Y. R. *Nature* **1989**, *337*, 519.
- Guyot-Sionnest, P.; Hunt, J. H.; Shen, Y. R. *Phys. Rev. Lett.* **1987**, *59*, 1597.
- MacPhail, R. A.; Strauss, H. L.; Snyder, R. G.; Elliger, C. A. *J. Phys. Chem.* **1984**, *88*, 334.
- Harris, A. L.; Chedney, C. E. D.; Levinos, N. J.; Loiacono, D. N. *Chem. Phys. Lett.* **1987**, *141*, 350.
- Bain, C. D.; Davies, P. B.; Ong, T. H.; Ward, R. N. *Langmuir* **1991**, *7*, 1563.
- Zhuang, X.; Miranda, P. B.; Kim, D.; Shen, Y. R. *Phys. Rev. B* **1999**, *59*, 12632.
- Hirose, C.; Akamatsu, N.; Domen, K. *Appl. Spectrosc.* **1992**, *6*, 1051.
- Wang, H. F.; Gan, W.; Lu, R.; Rao, Y.; Wu, B. H. *Int. Rev. Phys. Chem.* **2005**, *24*, 191.
- Hirose, C.; Akamatsu, N.; Domen, K. *J. Chem. Phys.* **1992**, *96*, 997.
- Hirose, C.; Yamamoto, H.; Akamatsu, N.; Domen, K. *J. Phys. Chem.* **1993**, *97*, 10064.
- Gray, D. E. *American Institute of Physics Handbook*; McGraw-Hill: New York, 1972.
- Hodgson, J. N. *Proc. Phys. Soc.* **1955**, *9B*, 593.
- Dean, J. A. *Lange's Handbook of Chemistry*; McGraw-Hill: New York, 1992.
- Cimatu, K.; Baldelli, S. *J. Phys. Chem. C* **2007**, *111*, 7137.
- Chaturvedi, S.; Rodriguez, J. A.; Hrbek, J. *J. Phys. Chem. B* **1997**, *101*, 10860.
- Mekhalif, Z.; Massi, L.; Guittard, F.; Geribaldi, S.; Delhalle, J. *Thin Solid Films* **2002**, *405*, 186.
- Wagner, C. D.; Riggs, W. M.; Davies, L. E.; Moulder, J. F.; Muilenberg, G. E. *Handbook of X-ray Photoelectron Spectroscopy*; Perkin-Elmer: Eden Prairie, MN, 1978.
- Widrig, C. A.; Chung, C.; Porter, M. D. *J. Electroanal. Chem.* **1991**, *310*, 355.
- Yang, D.-F.; Wilde, C.-P.; Morin, M. *Langmuir* **1997**, *13*, 243.
- Yang, D.-F.; Wilde, C.-P.; Morin, M. *Langmuir* **1996**, *12*, 6570.
- Hassan, H. H. *Appl. Surf. Sci.* **2001**, *174*, 201.
- Macdonald, J. R.; Johnson, W. B. *Fundamentals of Impedance Spectroscopy*; John Wiley & Sons: New York, 2005.
- Protsailo, L. V.; Fawcett, W. R. *Electrochim. Acta* **2002**, *45*, 3497.
- Boubour, E.; Lennox, R. B. *Langmuir* **2000**, *16*, 4222.
- Cimatu, K.; Baldelli, S. *J. Am. Chem. Soc.* **2006**, *128*, 16016.
- Sinapi, F.; Forget, L.; Delhalle, J.; Mekhalif, Z. *Appl. Surf. Sci.* **2003**, *212-213*, 464–471.
- Buck, M.; Eisert, F.; Fisher, J.; Grunze, M.; Träger, F. *Appl. Phys.* **1991**, *A53*, 552.
- Poirier, G. E.; Tarlov, M. *J. Phys. Chem.* **1995**, *99*, 10966.